Supplemental Material

Content:

Material and Methods

Material and Methods

Protein purification

Haspin and CLK1, both wild-type and all mutants, have been purified as described [13a, 19]. Briefly, the recombinant proteins were purified using Co^{2+}/Ni^{2+} affinity chromatography. For haspin, the His-tagged protein were subsequently purified by size-exclusion chromatography and the final protein was stored in 50 mM HEPES, pH 7.5, 300 mM NaCl, 0.5 mM TCEP. For CLK1, the histidine tag was removed by incubating the protein with TEV protease overnight. The cleaved CLK1 protein was separated by reverse purification on Ni^{2+} affinity chromatography, and subsequently size exclusion chromatography. The final CLK1 protein was stored in 30 mM HEPES, pH 7.5, 300 mM NaCl, 50 mM L-Arginine/L-Glutamate mix, 10 mM DTT, 1% glycerol.

Protein crystallization

All crystallization experiments were performed using sitting-drop vapour-diffusion method at 4 °C. For Haspin, the protein at ~12 mg/ml was incubated with 1 mM inhibitors, and the complexed crystals were obtained using the crystallization condition containing 51-63% MPD and 0.1M SPG buffer, pH 6.0-6.5. To obtain the inhibitor-CLK1 complex, apo crystals grew in 20% 1,2-propanediol, 5% glycerol and 0.1 M $NaKPO_4$ were soaked with inhibitor overnight.

Data collection and structure determination

All diffraction data were collected at Diamond Light Source, and processed using MOSFLM[20]. Scaling was performed using aimless from the CCP4 suite[21]. All structures were solved by molecular replacement using Phaser [22] and the deposited CLK1 and haspin structures (PDB entries 2VAG and 4OUC respectively) as models. All structures were subjected to one round of automated model building using *ARP/wARP[23]*, followed by iterative cycles of manual model building in COOT [24], alternated with refinement using REFMAC [25]. TLS definitions used in the final refining rounds were calculated using the TLSMD server [25]. The model quality and geometric correctness of all complexes was verified using MolProbity [26]. Statistics for data collection and structure refinement are summarized in Supplemental Table 11.

Thermal shift assays

Protein were diluted to 2 μM in a buffer containing 10 mM HEPES, pH 7.5 and 500 mM NaCl, and mixed with SYPRO Orange at 1000-fold dilution of the dye. The inhibitors were added at 10 μM final concentration. The DSF assay was performed using a Real-Time PCR Mx3005p machine (Stratagene) according to the protocol described previously [27].

Isothermal Titration Calorimetry

All proteins were exchanged into a suitable storage buffer. CLK1 at 100 μM was stored in 20 mM HEPES, pH 7.5, 300 mM NaCl, 50 mM L-arginine/L-glutamate mix and 0.5 mM TCEP. For haspin at 80 μM, the buffer containing 20 mM HEPES, pH 7.5, 250 mM NaCl and 0.5 mM TCEP was used for the wild-type protein, while the gatekeeper mutants were buffer exchanged into 30 mM HEPES, pH 7.5, 400 mM NaCl and 0.5 mM TCEP to increase their stabilities. Calorimetric measurements were carried out using a VP-ITC calorimeter (MicroCal) at 15 °C. For all experiments, the proteins were titrated into the reaction cell containing the compound. Integrated heat of titrations were manually corrected and analysed in Origin. Using a single binding site model, the obtained curve was fitted following a non-linear least-square minimization algorithm. The binding isotherms and the measured binding

enthalpy changes enabled the calculation of entropy changes (TΔS), Gibbs free energy (ΔG), the stoichiometry n and K_d.

Biolayer Interference

The binding kinetics were measured by Biolayer Interference method (BLI) using Octet RED384 system (*forté*BIO). For haspin, the experiments were performed in the buffer condition containing 20 mM HEPES, pH 7.5, 400 mM NaCl and 0.5 mM TCEP. For CLK1, the same buffer supplemented with 50 mM L-arginine/L-glutamate mix was used. Biotinylated proteins, prepared as previously described, were immobilized on streptavidin biosensors, which were subsequently quenched with L-biotin[28]. The interference patterns of association and dissociation events were measured through a time course of 600 seconds. The binding data were corrected using a double-referencing method, and the kinetics analyses were performed according to the manufacture protocol (*forté*BIO).

Surface Plasmon Resonance (SPR)

SPR experiments were performed in HBS-PE+ buffer on a Biacore T200 System (GE Healthcare). Biotinlyated wt and mutant Haspin (50 µg/ml in HBS-P+ buffer) were captured to a SA sensor chip (GE Healthcare) at typical densities of 2-5 kRU using the protocols provided by the manufacturer. Compounds were serially diluted in DMSO and transferred to assay buffer in a 1:100 dilution step to achieve their final test concentrations at a [DMSO] = 1%. For binding analysis, contact times of 60, 120, 240, 300 or 420 seconds were used depending on the kinetics assessed in preliminary tests. Likewise, dissociation times were adjusted to180, 900, 1500 or 3600 seconds, to achieve return of the SPR signals to baseline levels. To obtain kinetic and affinity parameters, sensorgrams (acquired at 10 Hz) were fitted using the BIAevaluation Software (GE Healthcare) to a 1:1 Langmuir model accounting for mass transport limitations. Steady state analysis was performed with the same software using a single site equilibrium binding equation.

Equilibrium und Kinetic probe competition assays (ePCA and kPCA)

ePCA and kPCA experiments were performed in Tris-HCl pH7.5, 150 mM NaCl, 0.01% Tween, 0.01% BSA, 2 mM DTT buffer as previously described for CDK2 in Schiele et al [17]. Biotinylated wt and mutant Haspin (4 nM in assay) were labelled at a molar ratio of 8:1 with SA-Terbium (Cisbio) as TR-FRET donor. Tracers 236 and 199 (Invitrogen) labelled with an Alexa 647 TR-FRET acceptor were respectively used as kinase specific probes at a final concentration of 100 nM.

Compounds were diluted and transferred to Greiner black small volume 384-well microtiter test plates as described[17]. For ePCA, tracer and labeled proteins were dispensed to the ready-to-use compound plates to a final volume of 5 µL and the mixture was incubated for 2 h prior to acquisition of the steady state TR-FRET ratiometric signals (665/620 nm) upon excitation at 337 nm. Normalized values were fitted to a logistic 4-parameter model using the Genedata Screener™ software, and Ki values calculated using the Cheng-Prusoff relationship. For kPCA, the tracer was dispensed to the ready-to-use compound plates prior to introducing them into the PHERAstar FS™ microtiter plate reader. Then the labeled proteins were added to wells to a final volume of 10 µL using the injector system of the instrument, and kinetic TR-FRET readings were made at time zero and every 10 seconds. Blank-subtracted kinetic traces were analyzed with a competitive binding kinetics model using the GraphPad Prism™ software as described [17].

Prior to compound testing, the steady state affinities of the probes were determined by equilibrium binding titrations (0 to 400 nM) on various Haspin concentrations (0 to 8 nM) with

end-point readings of the TR-FRET signals. The probes' association and dissociation kinetics were characterized by titrating them on 4 nM labeled Haspin (0.5 nM SA-Tb) and acquiring the TR-FRET signals in real time. Binding curves were fitted to the corresponding models with Graph Pad Prism™ in order to obtain the affinity and kinetic constants used as parameters in the Cheng-Prusoff and Motulsky and Mahan models.

Quantum mechanical interaction energy calculations

The energy contributions of the inhibitor-aromatic gatekeeper interaction were calculated using *ab initio* Møller–Plesset perturbation theory to second order (MP2). The Moeller-Plesset perturbation theory improves on the Hartree-Fock method by adding electron-correlation effects by means of Rayleigh-Schrödinger perturbation theory to different orders (second order in our case). The *Protein Preparation* wizard of the *Maestro* program of the *Schrodinger suite* (*Version 2015.r3*) was used to pre-process the X-ray crystallographic structures of the haspin-inhibitor complexes, to add missing side chains and to optimize the H-bond network. The *impref* utility of the *Maestro* was used for energy minimization using the *OPLS3* force field. The *impref* utility[29] first optimizes position of hydrogen atoms followed by all-atom minimization where non-hydrogen atoms are restrained with a harmonic potential using a force constant of 25 kcal/mol.Å^2. The coordinates of the inhibitor and the gatekeeper phenylalanine residue were extracted from these energy-minimized structures of haspin-inhibitor complexes. The termini of the phenylalanine residue were blocked with hydrogen atoms and their positions were optimized using the *OPLS3* force field in the *Maestro* program of the *Schrödinger suite* [30]. In the case of the gatekeeper mutants, the corresponding gatekeeper residues (tyrosine and threonine) were prepared in the same way.

The *def2TZVP* basis set was used for all calculations and effective core potentials (ECPs) were used for the iodine atom. *Ab initio* interaction energies at the MP2 level were calculated using the *GAMESS* software, and partitioned into their constituent interaction energy terms (see Equation 1) using the many body interaction energy decomposition scheme (EDS) described by *Góra et al.*[31]. In this scheme, the total interaction energy is calculated in a super-molecular approach as the difference between the total energy of a complex (here, of the inhibitor and the gatekeeper residue) and the sum of the energies of its isolated constituents. In all calculations, the complex centered basis set (CCBS) was used consistently and the results are therefore basis set superposition error (BSSE) free due to the full counterpoise correction.

$$E_{MP2} = E_{EL,MTP} + E_{EL,PEN} + E_{EX} + E_{DEL} + E_{CORR}$$

$$E_{SCF} = E_{EL,MTP} + E_{EL,PEN} + E_{EX} + E_{DEL}$$

Equation (1)

$$E_{HL} = E_{EL,MTP} + E_{EL,PEN} + E_{EX}$$

$$E_{EL} = E_{EL,MTP} + E_{EL,PEN}$$

As shown in Equation 1, the total interaction energy at the MP2 level of theory (E_{MP2}) includes the components of the Hartree-Fock interaction energy (E_{SCF}) and the second order Coulomb correlation correction term (E_{CORR}). This correlation term (E_{CORR}) includes the sec-

ond order intermolecular dispersion energy and the correlation corrections to the SCF components. The Hartree-Fock interaction energy (E_{SCF}) was partitioned into a first order Heitler-London component (E_{HL}) and a higher order Hartree-Fock delocalization interaction energy component (E_{DEL}), which encompasses the induction and the associated exchange effects. Because their separation could lead to a non-physical charge transfer, this component was not partitioned any further. The Heitler-London interaction energy component (E_{HL}) can be separated into the first-order electrostatic interactions (E_{EL}) of monomers (the inhibitor and the gatekeeper residue in our case) and the associated Heitler-London exchange repulsion energy (E_{EX}) due to the Fermi electron correlation effects. The electrostatic interaction energy (E_{EL}) was obtained as a first-order term in the polarization perturbation theory and the exchange repulsion term (E_{EX}) was calculated by subtracting the electrostatic interaction energy from the Heitler-London energy ($E_{EX} = E_{HL} - E_{EL}$). $E_{EL,MTP}$ refers to the electrostatic multipole component estimated from an atomic multipole expansion, $E_{EL,PEN}$ is the electrostatic penetration energy, calculated from the following expression: $E_{EL,PEN} = E_{EL} - E_{EL,MTP}$.

Binding free energy calculations

The molecular mechanics-generalized Born surface area (MM/GBSA) method was used to estimate the binding free energy of the inhibitors to haspin kinase. The initial coordinates of the haspin-inhibitor complexes were obtained from the co-crystallized structures (see Supplementary Figure 2). The *Protein Preparation* wizard of the *Schrodinger suite* (*Version 2015.r3*) was used for pre-processing of the structures, formation of disulfide bonds, addition of hydrogen atoms and assigning protonation states at pH 7.0. The *pmemd* module of the *Amber14* software suite [32] was used to perform the molecular dynamics (MD) simulations with the *ff14SB*[33] force field for protein. The *LEap* module of *AmberTools14* was used to construct the topologies of the haspin-inhibitor complexes. The ligand parameters were generated based on the generalized Amber force field (*GAFF*). To improve the description of charge, dipole moment and geometry of halogenated compounds in molecular mechanics calculations, the positive region (σ hole) centered on the halogen atom was represented by an extra-point charge (EP). This inclusion of an EP results in improved modeling of halogen-bonding in MD simulations. The force field parameters for this EP were taken from *Ibrahim et al.*[34]. For generation of the partial atomic charges for the ligands, the *RESP*[35] program was used to fit the atom-centered charges to the molecular electrostatic potential (MEP) grid computed by the *GAMESS* program. The system was centred and aligned with the axes to minimize the volume. The system was then solvated using the *TIP3P* water model[36] by immersing the protein-ligand complex in a cubic box of water molecules, such that the shortest distance between the edge of the solvation box and the complex is 10 Å. The net charge (-2e) of the system was then neutralized by adding Na^+ counter ions. For each system, energy minimization was performed in three 1500-cycle consecutive runs using the steepest descent minimization method followed by switching to the conjugate gradient method after 500 cycles. Gradually decreasing harmonic restraints with force constants of 500, 1 and 0 kcal/mol.Å^2 were used for non-hydrogen atoms in three consecutive runs. Energy minimization was followed by 1 nanosecond (*ns*) of gradual heating from 10 K to 300 K with harmonic restraints with a force constant of 50 kcal/mol.Å^2 acting on non-hydrogen atoms. Then

the system was equilibrated for 1 *ns* under *NPT* conditions at 300K, with heavy atoms (except solvent ions) harmonically restrained with a force constant of 50 kcal/mol.Å^2. This was followed by an *NPT* equilibration of 2 *ns* without any positional restraints. The potential energy function and atomic coordinates were calculated using a 2 femtoseconds (*fs*) time step. The *SHAKE*[37] algorithm was used to constrain all the bonds involving hydrogen atoms. The *Particle Mesh Ewald* (PME) method was used to calculate the electrostatic interactions. A cut-off of 10 Å was set for generating the non-bonded pair list and this pair list was updated every 100 steps. After equilibration, data were collected over a 6 *ns* simulation run for binding free energy calculations and 3000 sets of atomic coordinates were saved every 2 picoseconds (*ps*). MM/GBSA calculations of the binding free energy were performed using the *MMPBSA.py* module implemented in the *Amber14* analysis tools. A single-trajectory approach was used in which receptor, ligand and complex geometries were extracted from a single MD trajectory. All the ions and water molecules were stripped from the trajectory snapshots. A salt concentration of *0.15 M* and the Born implicit solvent model (*igb = 2*) were used. Each binding free energy was computed as the sum of a molecular mechanics term ($\triangle E_{gas}$), a Gibbs solvation term ($\triangle\triangle G_{solvation}$) and an entropic contribution ($T\triangle S_{solute}$). For the entropic contribution to binding free energy, we computed translational and rotational entropies with a rigid rotor model using the *MMPBSA.py* module. The calculation of vibrational entropies using normal-mode analysis with MMPBSA.py failed due to the inclusion of the EP in the force field. The free energy of binding for some of the derivatives is positive since vibrational and conformational entropy terms are neglected.

References

[1]   R. A. Copeland, D. L. Pompliano, T. D. Meek, *Nat Rev Drug Discov* **2006**, *5*, 730-739.

[2]   aS. Muller, A. Chaikuad, N. S. Gray, S. Knapp, *Nat Chem Biol* **2015**, *11*, 818-821; bA. Chaikuad, E. M. Tacconi, J. Zimmer, Y. Liang, N. S. Gray, M. Tarsounas, S. Knapp, *Nat Chem Biol* **2014**, *10*, 853-860; cZ. Zhao, H. Wu, L. Wang, Y. Liu, S. Knapp, Q. Liu, N. S. Gray, *ACS Chem Biol* **2014**, *9*, 1230-1241.

[3]   C. Pargellis, L. Tong, L. Churchill, P. F. Cirillo, T. Gilmore, A. G. Graham, P. M. Grob, E. R. Hickey, N. Moss, S. Pav, J. Regan, *Nat Struct Biol* **2002**, *9*, 268-272.

[4]   N. Willemsen-Seegers, J. C. Uitdehaag, M. B. Prinsen, J. R. de Vetter, J. de Man, M. Sawa, Y. Kawase, R. C. Buijsman, G. J. Zaman, *J Mol Biol* **2017**, *429*, 574-586.

[5]   E. V. Schneider, J. Bottcher, R. Huber, K. Maskos, L. Neumann, *Proc Natl Acad Sci U S A* **2013**, *110*, 8081-8086.

[6]   E. R. Wood, A. T. Truesdale, O. B. McDonald, D. Yuan, A. Hassell, S. H. Dickerson, B. Ellis, C. Pennisi, E. Horne, K. Lackey, K. J. Alligood, D. W. Rusnak, T. M. Gilmer, L. Shewchuk, *Cancer Res* **2004**, *64*, 6652-6659.

[7]   L. Englert, A. Biela, M. Zayed, A. Heine, D. Hangauer, G. Klebe, *Biochim Biophys Acta* **2010**, *1800*, 1192-1202.

[8]   P. Ayaz, D. Andres, D. A. Kwiatkowski, C. C. Kolbe, P. Lienau, G. Siemeister, U. Lucking, C. M. Stegmann, *ACS Chem Biol* **2016**, *11*, 1710-1719.

[9]   P. Schmidtke, F. J. Luque, J. B. Murray, X. Barril, *J Am Chem Soc* **2011**, *133*, 18903-18910.

[10]   aJ. M. Bradshaw, J. M. McFarland, V. O. Paavilainen, A. Bisconte, D. Tam, V. T. Phan, S. Romanov, D. Finkle, J. Shu, V. Patel, T. Ton, X. Li, D. G. Loughhead, P. A. Nunn, D. E. Karr, M. E. Gerritsen, J. O. Funk, T. D. Owens, E. Verner, K. A. Brameld, R. J. Hill, D. M. Goldstein, J. Taunton, *Nat Chem Biol* **2015**, *11*, 525-531; bR. M. Miller, V. O. Paavilainen, S. Krishnan, I. M. Serafimova, J. Taunton, *J Am Chem Soc* **2013**, *135*, 5298-5301; cM. Forster, A. Chaikuad, S. M. Bauer, J. Holstein,

M. B. Robers, C. R. Corona, M. Gehringer, E. Pfaffenrot, K. Ghoreschi, S. Knapp, S. A. Laufer, *Cell Chem Biol* **2016**, *23*, 1335-1340; dA. Chaikuad, P. Koch, S. Laufer, S. Knapp, *Angew Chem Int Ed Engl* **2017**.

[11] Q. Liu, Y. Sabnis, Z. Zhao, T. Zhang, S. J. Buhrlage, L. H. Jones, N. S. Gray, *Chem Biol* **2013**, *20*, 146-159.

[12] Z. Xu, Z. Yang, Y. Liu, Y. Lu, K. Chen, W. Zhu, *J Chem Inf Model* **2014**, *54*, 69-78.

[13] aJ. Eswaran, D. Patnaik, P. Filippakopoulos, F. Wang, R. L. Stein, J. W. Murray, J. M. Higgins, S. Knapp, *Proc Natl Acad Sci U S A* **2009**, *106*, 20198-20203; bF. Villa, P. Capasso, M. Tortorici, F. Forneris, A. de Marco, A. Mattevi, A. Musacchio, *Proc Natl Acad Sci U S A* **2009**, *106*, 20204-20209.

[14] O. Fedorov, F. H. Niesen, S. Knapp, *Methods Mol Biol* **2012**, *795*, 109-118.

[15] P. S. Ho, *Top Curr Chem* **2015**, *358*, 241-276.

[16] C. D. Tatko, M. L. Waters, *Org Lett* **2004**, *6*, 3969-3972.

[17] F. Schiele, P. Ayaz, A. Fernandez-Montalvan, *Anal Biochem* **2015**, *468*, 42-49.

[18] Y. Lu, Y. Wang, W. Zhu, *Phys Chem Chem Phys* **2010**, *12*, 4543-4551.

[19] A. N. Bullock, S. Das, J. E. Debreczeni, P. Rellos, O. Fedorov, F. H. Niesen, K. Guo, E. Papagrigoriou, A. L. Amos, S. Cho, B. E. Turk, G. Ghosh, S. Knapp, *Structure* **2009**, *17*, 352-362.

[20] A. G. Leslie, *Acta Crystallogr D Biol Crystallogr* **2006**, *62*, 48-57.

[21] M. D. Winn, C. C. Ballard, K. D. Cowtan, E. J. Dodson, P. Emsley, P. R. Evans, R. M. Keegan, E. B. Krissinel, A. G. Leslie, A. McCoy, S. J. McNicholas, G. N. Murshudov, N. S. Pannu, E. A. Potterton, H. R. Powell, R. J. Read, A. Vagin, K. S. Wilson, *Acta Crystallogr D Biol Crystallogr* **2011**, *67*, 235-242.

[22] A. J. McCoy, R. W. Grosse-Kunstleve, P. D. Adams, M. D. Winn, L. C. Storoni, R. J. Read, *J Appl Crystallogr* **2007**, *40*, 658-674.

[23] G. Langer, S. X. Cohen, V. S. Lamzin, A. Perrakis, *Nat Protoc* **2008**, *3*, 1171-1179.

[24] P. Emsley, K. Cowtan, *Acta Crystallogr D Biol Crystallogr* **2004**, *60*, 2126-2132.

[25] J. Painter, E. A. Merritt, *Acta Crystallogr D Biol Crystallogr* **2006**, *62*, 439-450.

[26] I. W. Davis, A. Leaver-Fay, V. B. Chen, J. N. Block, G. J. Kapral, X. Wang, L. W. Murray, W. B. Arendall, 3rd, J. Snoeyink, J. S. Richardson, D. C. Richardson, *Nucleic Acids Res* **2007**, *35*, W375-383.

[27] O. Fedorov, B. Marsden, V. Pogacic, P. Rellos, S. Muller, A. N. Bullock, J. Schwaller, M. Sundstrom, S. Knapp, *Proc Natl Acad Sci U S A* **2007**, *104*, 20523-20528.

[28] T. Keates, C. D. Cooper, P. Savitsky, C. K. Allerston, C. Phillips, M. Hammarstrom, N. Daga, G. Berridge, P. Mahajan, N. A. Burgess-Brown, S. Muller, S. Graslund, O. Gileadi, *N Biotechnol* **2012**, *29*, 515-525.

[29] G. M. Sastry, M. Adzhigirey, T. Day, R. Annabhimoju, W. Sherman, *J Comput Aided Mol Des* **2013**, *27*, 221-234.

[30] M. W. Schmidt, K. K. Baldridge, J. A. Boatz, S. T. Elbert, M. S. Gordon, J. H. Jensen, S. Koseki, N. Matsunaga, K. A. Nguyen, S. Su, T. L. Windus, M. Dupuis, J. A. Montgomery, *Journal of Computational Chemistry* **1993**, *14*, 1347-1363.

[31] R. W. Gora, W. A. Sokalski, J. Leszczynski, V. B. Pett, *J Phys Chem B* **2005**, *109*, 2027-2033.

[32] J. Lee, X. Cheng, J. M. Swails, M. S. Yeom, P. K. Eastman, J. A. Lemkul, S. Wei, J. Buckner, J. C. Jeong, Y. Qi, S. Jo, V. S. Pande, D. A. Case, C. L. Brooks, 3rd, A. D. MacKerell, Jr., J. B. Klauda, W. Im, *J Chem Theory Comput* **2016**, *12*, 405-413.

[33] J. A. Maier, C. Martinez, K. Kasavajhala, L. Wickstrom, K. E. Hauser, C. Simmerling, *J Chem Theory Comput* **2015**, *11*, 3696-3713.

[34] M. A. Ibrahim, *J Comput Chem* **2011**, *32*, 2564-2574.

[35]   F. Y. Dupradeau, A. Pigache, T. Zaffran, C. Savineau, R. Lelong, N. Grivel, D. Lelong, W. Rosanski, P. Cieplak, *Phys Chem Chem Phys* **2010**, *12*, 7821-7839.

[36]   W. L. C. Jorgensen, J.; Madura, J.; Impey, R. W.; Klein, M.L., , *J Chem Phys* **1983**, *79*, 926–935.

[37]   J. P. Ryckaert, G. Ciccotti, H. Berendsen, *J Comput Phys* **1977**, *23*, 327–341.

[38]   L. Cavallo, J. Kleinjung, F. Fraternali, *Nucleic Acids Res* **2003**, *31*, 3364-3366.

Supplemental Figure S1
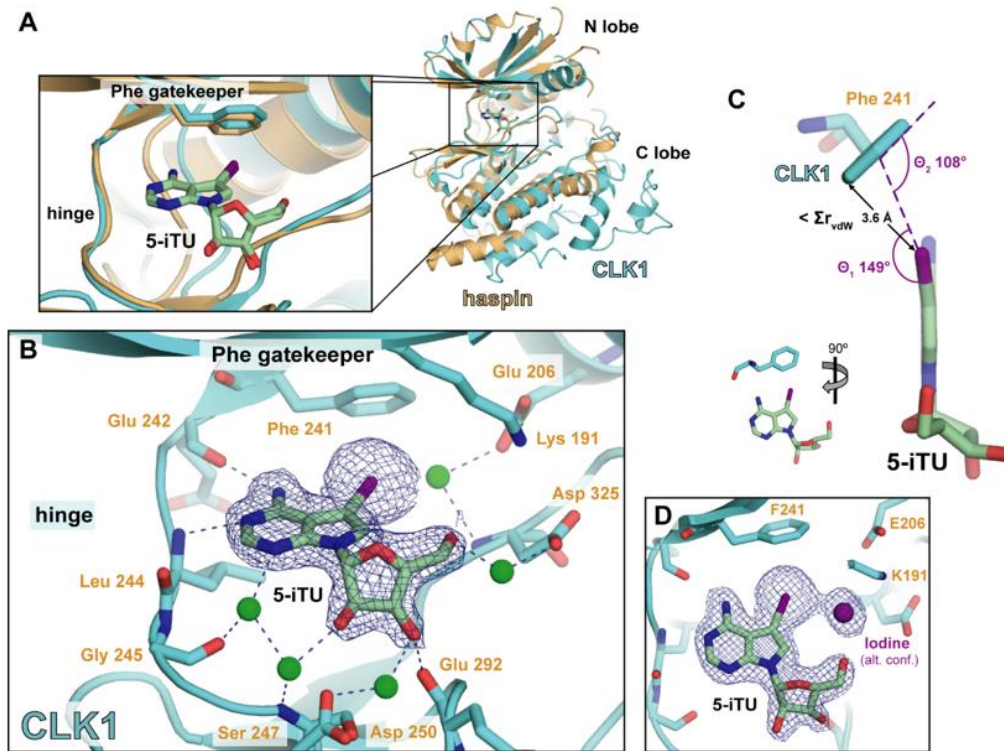
Supplemental Figure S1. The binding mode of 5-iTU is maintained in CLK1. (**A**) Superimposition of the structures of CLK1 and haspin (PDB ID: 4OUC) in complex with 5-iTU, showing that the binding mode is conserved. (**B**) Co-crystal structure of CLK1 and 5-iTU, highlighting interacting amino acid residues and the Phe gatekeeper. Water molecules are represented as green spheres, hydrogen bonds within 3 Å as blue dashed lines. Relevant atoms are colored as follows: oxygen – red, nitrogen – blue and iodine – purple. |2Fo|-|Fc | omitted electron density map is contoured at 3σ level. (**C**) Geometric measures of the putative π-X bond. (**D**) |2Fo|-|Fc | omitted electron density map contoured at 1σ level, showing alternative conformation of delocalized iodine in binding pocket.

Supplemental Figure S2
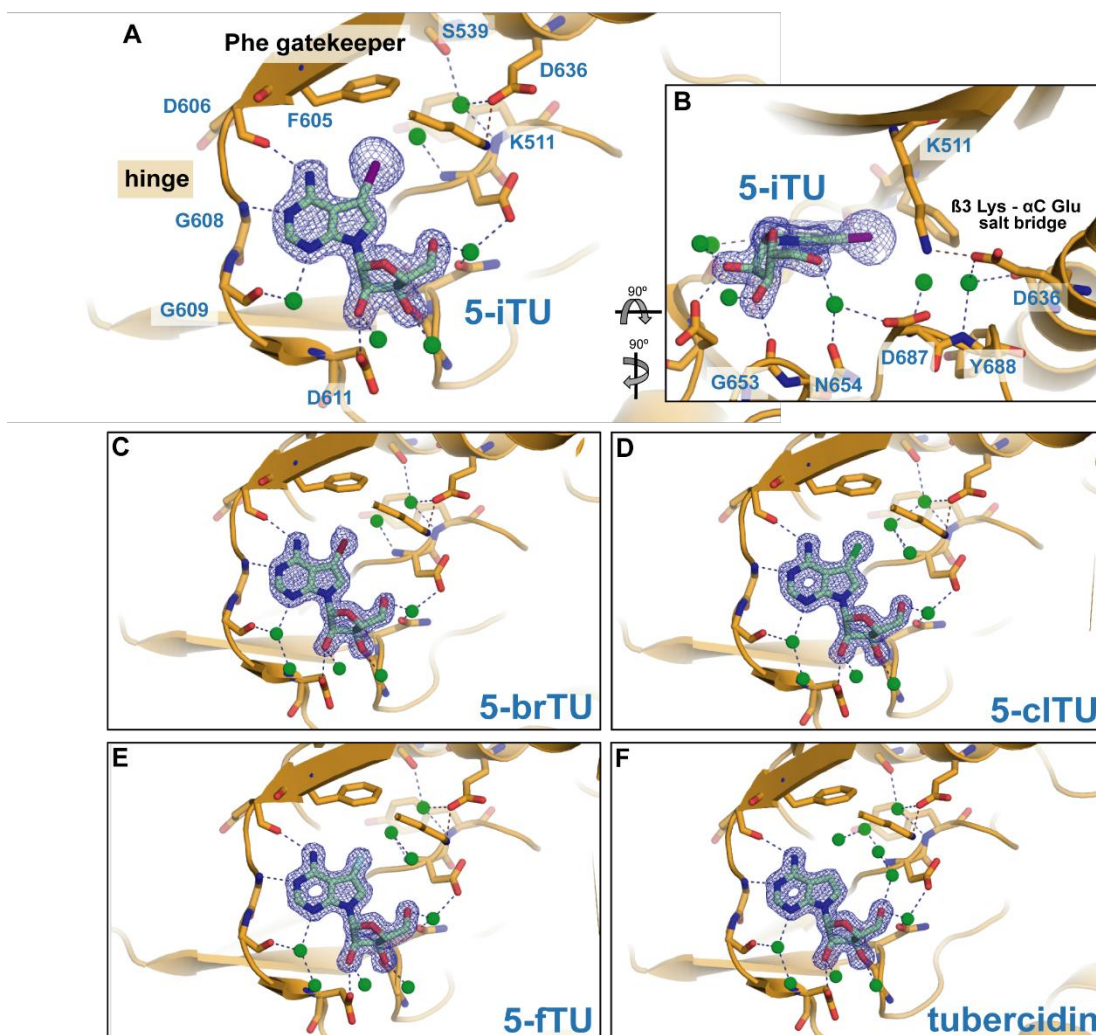
Supplemental Figure S2 - Structural studies of haspin in complex with the halogenated derivatives. (**A-B**) Co-crystal structure of haspin and 5-iTU, showing the ATP-competitive binding mode for the inhibitor. Interacting residues and the Phe gatekeeper are highlighted. Water molecules are represented as green spheres, hydrogen bonds within 3 Å as blue dashed lines. Relevant atoms are colored as follows: oxygen – red, nitrogen – blue and iodine – purple. |2Fo|-|Fc | omitted electron density map is contoured at 3σ level. (**C-F**) Co-crystal structures of haspin and different derivatives (see blue label), representation equivalent to (A). Bromine atom is shown in dark red, chlorine atom in green and fluorine atom in cyan.

Supplemental Figure S3 - 5-iTU-haspin binding site is maintained in the absence of an aromatic gatekeeper residue. (**A**) Superimposition of co-crystal structures of wild-type haspin (orange), haspin[F605Y] (slate) and haspin[F605T] (cyan) in complex with 5-iTU, showing that the binding modus is maintained in gatekeeper mutants. (**B**) Similar to (**A**), highlighting relevant residues in the binding pocket. Water molecules are shown as spheres and numbered from 1-5. (**C**) Co-crystal structure of haspin[F605T] in complex with 5-iTU. Water molecules are represented as green spheres and hydrogen bonds within 3 Å as blue dashed lines. Relevant atoms are coloured as follows: oxygen – red, nitrogen – blue and iodine – purple. |2Fo|-|Fc | omitted electron density map is contoured at 3σ level. (**D**) Same as (**C**), showing the co-crystal structure of haspin[F605Y] in complex with 5-iTU.
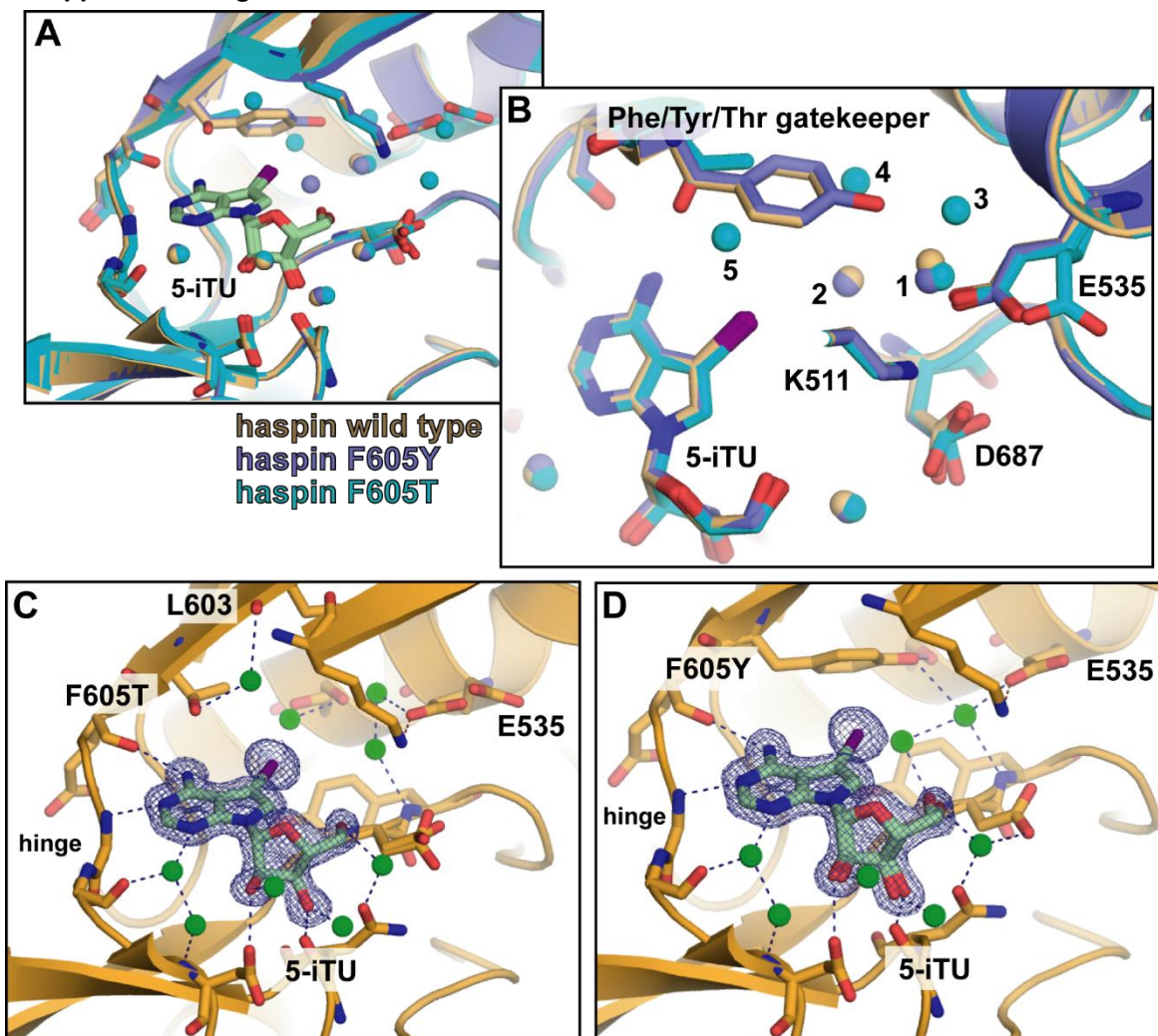
Supplemental Figure S4
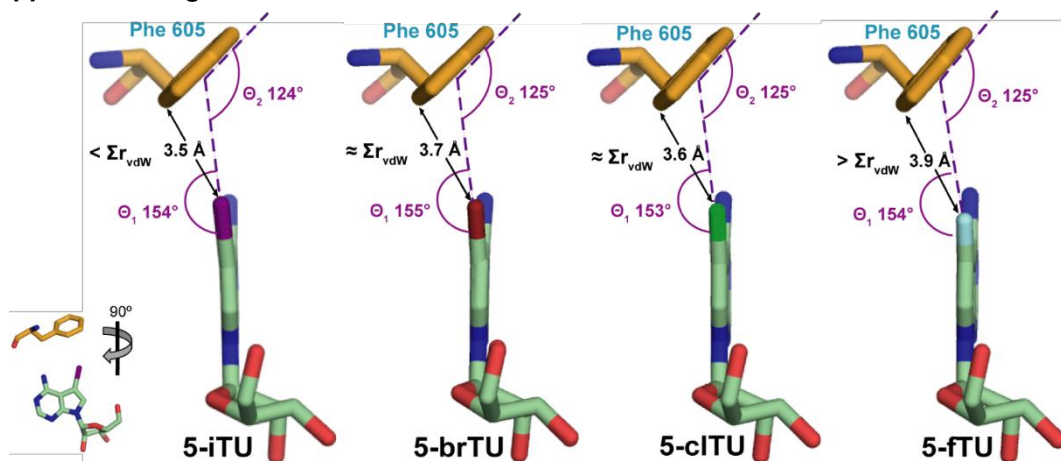
Supplemental Figure S4. Geometric measures of putative halogen-π-bonds. Overview of the halogenated derivatives approaching the aromatic ring of the Phe gatekeeper residue in haspin. The distance between the halogen and the closest carbon atom of the aromatic ring was measured and compared with the sum of the van der Waals radii ($\sum r_{vdW}$). Θ_1 is the angle between C-X bond to the centre of the phenylalanine aromatic group (C-X···π), while Θ_2 is the angle of the halogen to the plane of phenylalanine aromatic ring (X···π-C).

Supplemental Figure S5
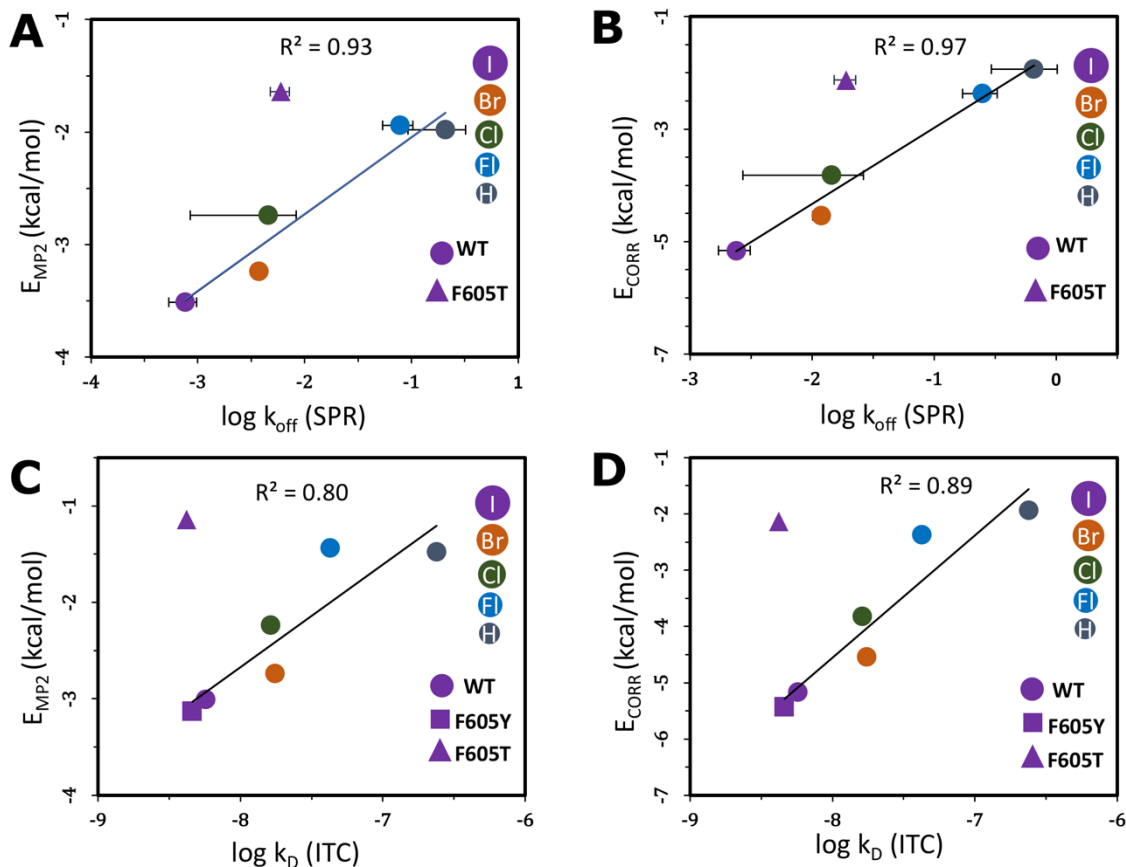
Supplemental Figure S5 – Correlation plots of computed quantum mechanical energies against experimental binding parameters. A) Second-order Møller–Plesset interaction energy (E_{MP2}) between the tubercidin derivatives and the gatekeeper residue versus the experimental (SPR) dissociation rate constants (k_{off}) of the tubercidin derivatives. B) The second-order correlation correction energy term (E_{CORR}) for the interaction between the tubercidin derivatives and the gatekeeper residue versus the experimental (SPR) dissociation rate constants (k_{off}) of the tubercidin derivatives This correlation energy (E_{CORR}) includes second-order intermolecular dispersion interactions and the correlation corrections to the Hartree-Fock (HF) energy. C) Second-order Møller–Plesset interaction energy (E_{MP2}) between tubercidin derivatives and gatekeeper residue versus the experimental (ITC) binding affinities (k_D) of the tubercidin derivatives. D) Second-order correlation correction energy term (E_{CORR}) for the interaction between the tubercidin derivatives and the gatekeeper residue versus the experimental (ITC) binding affinities (k_D) of the tubercidin derivatives. The correlation coefficients (R^2) and the linear fits were computed omitting the outlier data points for the F605T mutant. The error bars for the K_D (ITC) values are smaller than the size of the data point symbols.

Supplemental Table S1. DSF results for 5-iTU against 137 kinases. All results are listed with decreasing melting temperature shifts (ΔT_m). The gatekeeper residues (GK) of the kinases were determined by sequence alignment and analysis of the structures for hits with $\Delta T_m > 2^\circ$.

Kinase	ΔT_m	GK	Kinase	ΔT_m	GK	Kinase	ΔT_m	Kinase	ΔT_m
Haspin	11.40	Phe	TTK	2.20	Met	MAPK2TG	0.79	CAMK1G	0.20
DYRK2	10.38	Phe	RSK4	2.20	Leu	GRK1	0.76	CAMK1D	0.20
CLK4	9.59	Phe	AMPK1	2.19	Met	MYLK	0.73	CDPK1PF	0.12
CLK1	8.60	Phe	PIM2	2.04	Leu	CHEK2	0.70	VRK3	0.10
CLK3	7.50	Phe	GSK3β	2.00	Leu	CAMK2A	0.70	VRK2	0.10
CK1ε	5.90	Met	CK2α2	1.97	Phe	RIPK2	0.69	TOPK	0.10
DYRK1A	5.80	Phe	MAP2K2	1.90		MAPK9A	0.60	CAMK2B	0.10
CLK2	5.20	Phe	PRKCL1	1.83		CAMK2G	0.60	AAK1	0.09
CDK2	4.98	Phe	ITK	1.78		BMP2K	0.60	ADRBK2	0.03
MST3	4.96	Met	STK38	1.70		RPS6KA1	0.50	BMX	0.02
DRAK2	4.84	Leu	SNF1LK	1.70		AMPKA2	0.50	PRKG2	0.00
LOK	4.70	Ile	RPS6KA2	1.70		LOC340156	0.48	PDK1	0.00
YSK1	4.30	Met	RIOK2	1.70		ADRBK1	0.48	NLK	-0.10
SLK	4.20	Ile	PRKCL2	1.70		MAPK13	0.46	MAP2K6	-0.10
CAMK4	3.75	Leu	MERTK	1.70		TEC	0.45	NEK6	-0.20
AMPKα2	3.58	Met	PDPK1	1.69		CDKL2	0.43	CDK6	-0.20
MPSK1	3.40	Leu	RPS6KA3	1.66		NEK7	0.40	PKMYT1	-0.22
CK1γ2	3.30	Leu	PRKCZ	1.56		NEK2	0.40	DDR1	-0.38
PHKγ2	3.24	Phe	MAPK3A	1.50		MAP3K5	0.40	CDC42BPG	-0.38
RIPK3	3.21	Thr	TLK1	1.45		JAK1	0.40	MAPK11	-0.40
CDKL5	3.16	Phe	PIM1	1.40		SRPK2	0.39	CAMK2D	-0.40
MST1	3.10	Met	NEK11	1.31		CDPK1PV	0.39	DMPK1	-0.58
STK33	3.06	Leu	PRKACA	1.30		BRK1	0.39	CDC42BPAB	-0.74
PLK4	2.90	Leu	PIM3	1.30		MAPK2PF	0.35		
DAPK3	2.90	Leu	GAK	1.30		CDC42BPB	0.35		
DRAK1	2.80	Leu	CDKL3	1.30		ZAK	0.34		
PFTAIRE1	2.71	Phe	MYLK2	1.28		DCAMKL	0.33		
CDK8	2.71	Phe	IKBKB	1.25		YANK3	0.30		
MST2	2.70	Met	PRKD2	1.24		PRKX	0.28		
ERK3	2.70	Gln	PCTK1	1.11		TYK2	0.27		
CSNK1γ3	2.70	Leu	NEK9	1.06		MSSK1	0.26		
PRKCN	2.62	Met	CSNK2A1	1.05		LIMK1	0.26		
NDR2	2.60	Met	TNIK	1.00		SRPK1	0.25		
CK1γ1	2.50	Leu	PRKG1	1.00		VRK1	0.20		
QIK	2.41	Ile	NEK1	0.96		TYRO3	0.20		
STK39	2.40	Met	PCTK2	0.83		PAK6	0.20		
MEK1	2.29	Met	MST4	0.80		PAK5	0.20		
GRK5	2.22	Leu	YANK1	0.79		CDKL1	0.20		

Supplemental Table 2. BLI and ITC data.

Supplemental Table S2A - Summary of ITC and BLI data for 5-iTU in complex with CLK1 and CLK3

5-iTU vs	n	ITC data ΔH kcal/mol	$T\Delta S$ kcal/mol	ΔG kcal/mol	K M^{-1}	K_d nM	BLI data k_{on} $M^{-1}\,s^{-1}$	k_{off} s^{-1}	Resi-denceTime
CLK1	0.96	-16.66 (± 0.09)	-5.94	-10.72	1.39e+8 (± 1.99e+7)	**7.2** (±1.0)	10.9e+4 (±8.48e+3)	3.14e-4 (±1.06e-5)	**53.1 min** (±6.3 min)
CLK3	1.00	-12.04 (± 0.05)	-2.44	-9.60	1.91e+7 (± 1.28e+6)	**52.4** (±3.5)	-	-	-

Supplemental Table S2B- Summary of ITC and BLI data for halogenated derivatives against haspin

haspin vs	n	ITC data ΔH kcal/mol	$T\Delta S$ kcal/mol	ΔG kcal/mol	K M^{-1}	K_d nM	BLI data k_{on} $M^{-1}\,s^{-1}$	k_{off} s^{-1}	Resi-denceTime
tubercidin	0.95	-16.95 (± 0.10)	-8.21	-8.74	4.18e+6 (±1.74e+5)	**239.2** ±10.0)	9.56e+4 (±1.45e+3)	4.74e-2 (±6.72e-4)	**21.1 sec** (±0.3 sec)
5-FTu	1.00	-18.10 (± 0.07)	-8.39	-9.71	2.34e+7 (±1.56e+6)	**42.7** (±2.8)	9.26e+4 (±9.71e+2)	6.32e-3 (±4.44e-5)	**2.6 min** (±1.1 sec)
5-ClTu	0.98	-21.54 (± 0.06)	-11.27	-10.27	6.14e+7 (±3.29e+6)	**16.3** (±0.9)	9.00e+4 (±5.94e+2)	9.22e-4 (±8.00e-6)	**18.1 min** (±9.4 sec)
5-BrTu	1.00	-22.50 (±0.07)	-12.28	-10.22	5.70e+7 (±4.26e+6)	**17.5** (±1.3)	9.57e+4 (±3.36e+2)	6.42e-4 (±5.76e-5)	**25.9 min** (±2.3 min)
5-ITu	0.96	-23.40 (±0.07)	-12.53	-10.87	1.75e+8 (±1.66e+7)	**5.7** (±0.5)	9.59e+4 (±5.61e+2)	2.76e-4 (±5.96e-6)	**60.4 min** (±1.3 min)

Supplemental Table S2C- Summary of ITC and BLI data for haspin gatekeeper mutants against 5-iTU

5-iTU vs	n	ITC data ΔH kcal/mol	$T\Delta S$ kcal/mol	ΔG kcal/mol	K M^{-1}	K_d nM	BLI data k_{on} $M^{-1}\,s^{-1}$	k_{off} s^{-1}	Resi-denceTime
F605Y	0.96	-22.26 (± 0.05)	-11.27	-10.99	2.34e+7 (± 1.56e+6)	**4.6** (±0.3)	11.2e+4 (±1.45e+3)	4.29e-4 (±8.87e-6)	**38.9 min** (±48 sec)
F605H	0.98	-20.35 (± 0.05)	-9.42	-10.93	6.14e+7 (± 3.29e+6)	**5.1** (±0.3)	-	-	-
F605M	0.94	-22.09 (±0.04)	-10.89	-11.20	5.70e+7 (± 4.26e+6)	**3.2** (±0.2)	-	-	-
F605L	0.97	-23.35 (±0.04)	-12.36	-10.99	1.75e+8 (± 1.66e+7)	**4.6** (±0.4)	-	-	-
F605T	0.93	-20.48 (±0.03)	-9.42	-11.06	1.75e+8 (± 1.66e+7)	**4.2** (±0.4)	12.4e+4 (±6.22e+2)	1.23e-3 (±6.54e-6)	**13.5 min** (±4.3 sec)
F605Q	0.98	-23.23 (±0.04)	-12.56	-10.67	1.75e+8 (± 1.66e+7)	**8.0** (±0.8)	-	-	-

Supplemental Table S3. Summary of SPR data for haspin wild-type and F605T mutant against tubercidin derivatives

A wild-type (F605)

	K_D eq (nM)	K_D kin (nM)	k_{on} (M⁻¹s⁻¹)	k_{off} (s⁻¹)
tubercidin (hydrogen)	2560 ±1230	2910 ±707	1.96×10^5 ±1.59×10^5	6.57×10^{-1} ±3.62×10^{-1}
5-fTU (fluoride)	155 ±91	79.3 ±35.9	2.06×10^6 ±2.07×10^6	2.49×10^{-1} ±0.79×10^{-1}
5-clTU (Chloride)	6.6 ±2.8	4.9 ±2.8	2.79×10^6 ±1.26×10^6	1.45×10^{-2} ±1.18×10^{-2}
5-brTU (Bromide)	2.6 ±0.3	1.3 ±0.3	9.71×10^6 ±2.67×10^6	1.19×10^{-2} ±0.18×10^{-2}
5-iTU (iodide)	0.8 ±0.2	0.3 ±0.1	9.39×10^6 ±2.03×10^6	2.40×10^{-3} ±0.70×10^{-3}
fold difference				
H to I	↓ 3200	↓ 9700	↑ 48	↓ 274
F to I	↓ 194	↓ 264	↑ 5	↓ 104

B mutant F605T

	K_D eq (nM)	K_D kin (nM)	k_{on} (M⁻¹s⁻¹)	k_{off} (s⁻¹)
tubercidin (hydrogen)	5410 ±2180	6870	5.53×10^4 ±1.25×10^4	3.29×10^{-1} ±0.68×10^{-1}
5-fTU (fluoride)	1660 ±661	1490 ±258	1.22×10^5 ±0.40×10^5	1.76×10^{-1} ±0.33×10^{-1}
5-clTU (Chloride)	166 ±81	154 ±44	7.47×10^5 ±1.00×10^5	1.12×10^{-1} ±0.25×10^{-1}
5-brTU (Bromide)	53.3 ±24.6	46.3 ±9.1	1.07×10^6 ±0.12×10^6	4.88×10^{-2} ±0.77×10^{-2}
5-iTU (iodide)	12.8 ±5.1	12.0 ±2.2	1.61×10^6 ±0.44×10^6	1.89×10^{-2} ±0.38×10^{-2}
fold difference				
H to I	↓ 422	↓ 573	↑ 29	↓ 17
F to I	↓ 129	↓ 124	↑ 13	↓ 9

C wild-type (F605) vs mutant F605T on 5-iTU

fold difference				
	K_D eq (nM)	K_D kin (nM)	k_{on} (M⁻¹s⁻¹)	k_{off} (s⁻¹)
5-iTU	↓ 16	↓ 40	↑ 6	↓ 8

Supplemental Table S4. Solvent accessible surface area of ordered water molecules in the binding pocket. The Solvent Accessible Surface Area (SASA) of water molecules W1-W5 (as shown in Supplemental Figure 3), the nitrogen atom of the ε-amino group of K511 (NZ) and the closest C atom of the aromatic ring of F605 (CD1), was obtained by the POPS server, using a probe with 1.4 Å radius[38]. The structures with the halogenated derivatives are compared with the haspin apo-structure (PDB ID: 2WB8).

SASA (Å^2)	haspin/ 5-iTU	haspin/ 5-brTU	haspin/ 5-clTU	haspin/ 5-fTU	haspin/ tubercidin	Apo haspin
W1	2.13	2.20	1.88	1.84	1.74	1.34
W2	3.14	2.69	2.64	2.64	1.70	2.06
W3	-	-	4.03	3.94	3.50	5.07
W4	-	-	-	-	3.47	-
W5	-	-	-	-	3.21	-
NZ (K511)	4.56	4.88	3.80	3.46	4.02	4.23
CD$_1$ (F605)	1.49	1.39	1.44	1.41	1.37	1.31

Supplemental Table S5. Measured geometric parameters between the halogens and the Phe gatekeeper

	CLK1 / 5-iTU	haspin / 5-iTU	haspin / 5-brTU	haspin / 5-clTU	haspin / 5-fTU	Preferred geometry of X-bonds
Distance between halogen and closest C atom of gatekeeper	3.58 Å ± 0.28 Å ($< \sum r_{vdW}$)	3.52 Å ± 0.18 Å ($< \sum r_{vdW}$)	3.68 Å ± 0.19 Å ($\approx \sum r_{vdW}$)	3.61 Å ± 0.17 Å ($\approx \sum r_{vdW}$)	3.85 Å ± 0.17 Å ($> \sum r_{vdW}$)	$\leq \sum r_{vdW}$
Sum of van der Waals radii	3.68 Å	3.68 Å	3.60 Å	3.45 Å	3.20 Å	-
Angle Θ_1	149.5º	153.7º	154.7 º	153.3º	154.0º	$\approx 160º - 165º$
Angle Θ_2	108.0º	124.0º	125.1º	124.6º	125.3º	$\approx 120º$ ($\approx 90º$ for π-x-bond)

Supplemental Table S6 - Total interaction energy [*kcal. mol⁻¹*] between tubercidin derivatives and gatekeeper Phe 605 residue at consecutively increasing levels of quantum mechanical theory, see equation 1. E_{EL} is the electrostatic energy only, E_{HL} includes the Heitler-London energy, E_{SCF} includes the Hartree-Fock energy as well, and E_{MP2} is the full Moeller-Plesset second order energy. k_{off} values were measured by SPR and BLI, and K_D values were measured by SPR and ITC.

Inhibitor	log k_{off} (SPR)	log k_{off} (BLI)	log K_D (SPR)	log K_D (ITC)	E_{EL}	E_{HL}	E_{SCF}	E_{MP2}
5-iTU	-2.62	-3.56	-9.10	-8.24	-1.85	2.79	2.15	-3.01
5-brTU	-1.92	-3.19	-8.59	-7.76	-1.09	2.22	1.78	-2.74
5-clTU	-1.84	-3.04	-8.18	-7.79	-0.52	1.91	1.58	-2.24
5-fTU	-0.60	-2.20	-6.81	-7.37	0.17	1.15	0.94	-1.44
tubercidin	-0.18	-1.32	-5.59	-6.62	-0.09	0.65	0.47	-1.48
Pearson Correlation coefficient (R^2) with log k_{off} (SPR)					0.82	-0.98	-0.98	0.93
Pearson Correlation coefficient (R^2) with log k_{off} (BLI)					0.82	-0.98	-0.99	0.91
Pearson Correlation coefficient (R^2) with log K_D (SPR)					0.71	-0.97	-0.99	0.87
Pearson Correlation coefficient (R^2) with log K_D (ITC)					0.79	-0.96	-0.97	0.86

Supplemental Table S7 - Contribution of the different interaction energy terms to the total interaction energy, E_{MP2} [*kcal. mol⁻¹*], between tubercidin derivatives and the gatekeeper Phe 605 residue. See equation 1 for the definition of the terms. $E_{EL,MTP}$ is the electrostatic multipole term, $E_{EL,PEN}$ is the penetration electrostatic term, E_{EX} is the exchange term, E_{DEL} is the delocalization term, and E_{CORR} is the correlation energy term. k_{off} values were measured by SPR and BLI, and K_D values were measured by SPR and ITC.

Inhibitor	log k_{off} (SPR)	log k_{off} (BLI)	log K_D (SPR)	log K_D (ITC)	$E_{EL,MTP}$	$E_{EL,PEN}$	E_{EX}	E_{DEL}	E_{CORR}
5-iTU	-2.62	-3.56	-9.10	-8.24	2.48	-4.33	4.63	-0.64	-5.16
5-brTU	-1.92	-3.19	-8.59	-7.76	1.03	-2.12	3.30	-0.42	-4.54
5-clTU	-1.84	-3.04	-8.18	-7.79	-0.21	-0.32	2.44	-0.34	-3.82
5-fTU	-0.60	-2.20	-6.81	-7.37	0.13	0.04	0.97	-0.21	-2.37
tubercidin	-0.18	-1.32	-5.59	-6.62	-0.07	-0.01	0.74	-0.18	-1.94
Pearson Correlation coefficient (R^2) with log k_{off} (SPR)					-0.55	0.69	-0.94	0.89	0.98
Pearson Correlation coefficient (R^2) with log k_{off} (BLI)					-0.68	0.76	-0.92	0.88	0.96
Pearson Correlation coefficient (R^2) with log K_D (SPR)					-0.49	0.61	-0.88	0.80	0.95
Pearson Correlation coefficient (R^2) with log K_D (ITC)					-0.70	0.76	-0.90	0.88	0.92

Supplemental Table S8 - Total interaction energy [*kcal. mol^{-1}*] between tubercidin derivatives and gatekeeper Phe 605 residue at consecutively increasing levels of quantum mechanical theory, see equation 1. E_{EL} is the electrostatic energy only, E_{HL} includes the Heitler-London energy, E_{SCF} includes the Hartree-Fock energy as well, and E_{MP2} is the full Moeller-Plesset second order energy. k_{off} values were measured by SPR and BLI, and K_D values were measured by SPR and ITC. The correlation coefficient was calculated only for k_{off} and K_D values measured by BLI and ITC, respectively, as there were no SPR data available for the F605Y mutant.

System	log k_{off} (SPR)	log k_{off} (BLI)	log K_D (SPR)	log K_D (ITC)	E_{EL}	E_{HL}	E_{SCF}	E_{MP2}
Wild type	-2.62	-3.56	-9.10	-8.24	-1.85	2.79	2.15	-3.01
F605Y	ND	-3.37	ND	-8.34	-2.27	3.01	2.30	-3.13
F605T	-1.72	-2.91	-7.89	-8.38	-0.78	1.38	0.99	-1.14
Pearson Correlation coefficient (R^2) with log k_{off} (BLI)					0.84	-0.91	-0.92	0.94
Pearson Correlation coefficient (R^2) with log K_D (ITC)					-0.52	0.64	0.65	-0.69

Supplemental Table S9 - Contribution of the different interaction energy terms to the total interaction energy, E_{MP2} [*kcal. mol^{-1}*] between 5-iTU and the gatekeeper residue for the wild type and the two mutants. See equation 1 for the definition of the terms. $E_{EL,MTP}$ is the electrostatic multipole term, $E_{EL,PEN}$ is the penetration electrostatic term, E_{EX} is the exchange term, E_{DEL} is the delocalization term, and E_{CORR} is the correlation energy term. k_{off} values were measured by SPR and BLI, and K_D values were measured by SPR and ITC. The correlation coefficient was calculated only for k_{off} and K_D values measured by BLI and ITC, respectively, as there were no SPR data available for the F605Y mutant.

System	log k_{off} (SPR)	log k_{off} (BLI)	log K_D (SPR)	log K_D (ITC)	$E_{EL,MTP}$	$E_{EL,PEN}$	E_{EX}	E_{DEL}	E_{CORR}
Wild type	-2.62	-3.56	-9.10	-8.24	2.48	-4.33	4.63	-0.64	-5.16
F605Y	ND	-3.37	ND	-8.34	0.41	-2.68	5.28	-0.71	-5.43
F605T	-1.72	-2.91	-7.89	-8.38	-6.97	6.19	2.17	-0.39	-2.13
Pearson Correlation coefficient (R^2) with log k_{off} (BLI)					-1.00	0.99	-0.88	0.88	0.93
Pearson Correlation coefficient (R^2) with log K_D (ITC)					0.86	-0.82	0.58	-0.57	-0.68

Supplemental Table S10 - Binding free energies calculated using the MMGBSA approach for the binding of tubercidin derivatives with haspin.

Inhibitor	$\Delta E_{gas} + \Delta\Delta G_{solvation}$ (kcal/mol)	$T\Delta S_{MMGBSA}$ (kcal/mol)	ΔG_{MMGBSA} (kcal/mol)
5-iTU	-25.95 ± 2.93	-23.52 ± 0.02	-2.43 ± 2.95
5-brTU	-26.00 ± 2.75	-23.27 ± 0.02	-2.73 ± 2.77
5-clTU	-21.58 ± 3.33	-22.97 ± 0.02	1.39 ± 3.35
5-fTU	-20.31 ± 3.04	-22.83 ± 0.01	2.52 ± 3.05
tubercidin	-19.45 ± 2.87	-22.65 ± 0.02	3.20 ± 2.89

Supplemental Table S11 - Data collection and refinement statistics

	haspin-5- iTU	haspin-5-brTU	haspin-5-clTU	haspin-5-fTU	haspin-tu-bercidin	haspin^{F605Y}-5-iTu	haspin^{F605T}-5-iTu	CLK1-5-iTu
PDB IDs	**6G34**	**6G35**	**6G36**	**6G37**	**6G38**	**6G39**	**6G3A**	**6G33**
Data collection								
Space group	$P\,2_12_12_1$	$P\,2_12_12_1$	$P\,2_12_12_1$	$P\,2_12_12_1$	$P\,2_12_12_1$	$P\,2_12_12_1$	$P\,2_12_12_1$	$P\,121$
Wavelength (Å)	0.9794	0.9795	0.9794	0.9795	0.9794	0.9795	0.9795	1.0282
Cell dimensions								
a, b, c (Å)	78.6, 78.7, 79.7	78.3, 78.8, 79.4	77.7, 78.9, 79.8	78.7, 78.9, 79.6	78.6, 78.8, 80.0	78.8, 79.0, 79.5	78.4, 78.7, 79.8	56.2, 116.2, 91.0
α, β, γ (°)	90.0, 90.0, 90.0	90.0, 90.0, 90.0	90.0, 90.0, 90.0	90.0, 90.0, 90.0	90.0, 90.0, 90.0	90.0, 90.0, 90.0	90.0, 90.0, 90.0	90.0, 99.0, 90.0
Resolution (Å) [a]	23.98-1.76 (1.79-1.76)	23.87-1.55 (1.63-1.55)	23.78-1.46 (1.48-1.46)	23.80-1.48 (1.51-1.48)	24.05-1.43 (1.45-1.43)	22.01-1.45 (1.53-1.45)	22.01-1.43 (1.45-1.43)	29.34-2.05 (2.16-2.05)
R_{merge} [a]	0.087 (0.224)	0.073 (0.643)	0.075 (0.629)	0.149 (2.022)	0.102 (1.135)	0.060 (0.570)	0.122 (2.039)	0.092 (0.627)
$I\,/\,\sigma I$ [a]	13.9 (7.2)	10.8 (2.3)	12.3 (2.5)	9.9 (2.5)	8.6 (1.2)	14.2 (3.0)	11.3 (2.7)	8.2 (2.1)
Completeness (%)	98.1 (96.8)	99.8 (99.8)	99.8 (98.1)	100.0 (100.0)	99.9 (98.3)	98.3 (96.9)	99.8 (99.5)	99.9 (99.9)
CC1/2 [a]	0.994 (0.968)	0.996 (0.758)	0.996 (0.741)	0.994 (0.648)	0.994 (0.379)	0.997 (0.801)	0.995 (0.751)	0.997 (0.830)
Redundancy [a]	6.2 (6.5)	5.2 (5.2)	6.0 (5.5)	9.3 (9.2)	5.9 (4.2)	5.4 (5.4)	9.3 (9.5)	5.2 (5.1)
Unique reflections	48,665 (2,699)	71,557 (10,321)	85,664 (4,145)	83,206 (4,087)	92,144 (4,423)	86,860 (12,366)	91,424 (4,471)	72,225 (10,553)
Refinement								
R_{work}/R_{free}	0.138/0.174	0.160/0.183	0.149/0.176	0.148/0.167	0.143/0.165	0.158/0.175	0.150/0.175	0.188/0.218
No. atoms								
Protein	2,602	2,778	2,742	2,612	2,595	2,726	2,655	8,251
Inhibitor	21	42	53	20	19	42	25	120
Others[b]	249	336	253	220	293	356	236	346
B-factors								
Protein	21.45	27.38	21.82	19.59	21.52	23.86	20.65	26.74
5-ITu/derivative	16.85	18.87	26.56	13.66	14.84	16.47	15.37	27.75
Water/solvents	27.38	38.58	27.87	25.69	30.48	35.89	25.40	45.94
r.m.s. deviations[c]								
bond length (Å)	0.017	0.016	0.013	0.013	0.012	0.015	0.013	0.015
bond angles (°)	1.8	1.6	1.6	1.6	1.5	1.6	1.6	1.5
Ramachandran								
outliers (%)	0.0	0.0	0.0	0.3	0.0	0.0	0.0	0.0
favored (%)	98.48	98.85	98.55	98.48	98.78	98.84	98.51	97.7
Coordinate error (Luzzati plot)	0.18 A	0.19 A	0.17	0.17	0.17	0.17	0.18	0.28

[a] values in parentheses refer to the highest resolution shell.
[b] Others indicate water and solvent molecules

[c] r.m.s. deviations indicates root mean square deviations